Microwave-Assisted Topochemical Conversion of Layered Titanate Nanosheets to {010}-Faceted Anatase Nanocrystals for High Performance Photocatalysts and Dye-Sensitized Solar Cells

ARTICLE *in* CRYSTAL GROWTH & DESIGN · OCTOBER 2014

Impact Factor: 4.89 · DOI: 10.1021/cg501062r

7 AUTHORS, INCLUDING:

Chen Changdong
Kagawa University
6 PUBLICATIONS **24** CITATIONS
SEE PROFILE

Galhenage Asha Sewvandi
University of Moratuwa
8 PUBLICATIONS **33** CITATIONS
SEE PROFILE

Takafumi Kusunose
Kagawa University
116 PUBLICATIONS **1,261** CITATIONS
SEE PROFILE

Shunsuke Nakanishi
Kagawa University
107 PUBLICATIONS **562** CITATIONS
SEE PROFILE

CRYSTAL GROWTH & DESIGN

Article

pubs.acs.org/crystal

Microwave-Assisted Topochemical Conversion of Layered Titanate Nanosheets to {010}-Faceted Anatase Nanocrystals for High Performance Photocatalysts and Dye-Sensitized Solar Cells

Changdong Chen, Linfeng Xu, Galhenage A. Sewvandi, Takafumi Kusunose, Yasuhiro Tanaka, Shunsuke Nakanishi, and Qi Feng*

Department of Advanced Materials Science, Faculty of Engineering, Kagawa University, 2217-20 Hayashi-cho, Takamatsu 761-0396, Japan

Supporting Information

ABSTRACT: The {010}-faceted anatase nanocrystals with controllable crystal size and morphology were synthesized by microwave hydrothermal treatment of layered titanate nanosheet solutions. The nanostructures and formation reaction mechanism of TiO_2 nanocrystals were investigated using X-ray diffraction, field emission scanning electron microscopy, transmission electron microscopy, and selected-area electron diffraction. Their photocatalytic behavior and dye-sensitized solar cell (DSSC) performance were studied and compared with [111]-faceted anatase nanocrystals and anatase nanocrystals without a specific facet on the surface. There are two kinds of reactions in the formation process of the anatase nanocrystals. One is an in situ topochemical conversion reaction of layered titanate structure to anatase structure, and another is the dissolution−deposition reaction on the particle surface. The microwave hydrothermal process is suitable to control the structural conversion reaction for uniform the crystal size and morphology due to its uniform heating mechanism. The UV−visible spectrum results revealed that the bandgap of the TiO_2 nanocrystals was enhanced in the order of nanocrystal without specific facet < [111]-faceted nanocrystal < {010}-faceted nanocrystal, which corresponded to their photocatalytic activities. The DSSC performance also was enhanced in the same order, suggesting that the {010}-faceted nanocrystals are promising for the high performance DSSCs.

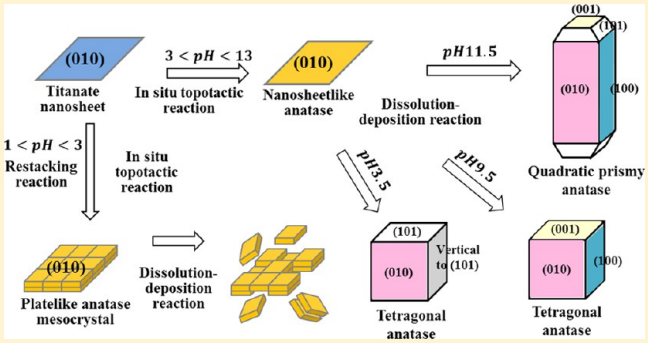

INTRODUCTION

Titanium dioxide (TiO_2) is one of the most important functional materials and has attracted much attention in the last decades due to its excellent photocatalytic[1−3] and dye-sensitized solar cell (DSSC) performances,[4−6] low cost, and nontoxicity. To improve photocatalytic performance of TiO_2 materials, a large number of studies have been implemented on the syntheses of the nanocrystals and nanostructured materials, extending the light absorption region to visible light by nitrogen-doping,[7] and synthesis of TiO_2 heterojunction materials to improve charge separation ability.[8] TiO_2 as a primary material impacts dye adsorption and photoelectron transport, which strongly affect the performance of DSSCs.[9] In fact, the crystal structure, crystallinity, crystal size, morphology, and crystal surface structure, such as crystal facet exposed on the surface of TiO_2 materials, can affect photocatalytic and photovoltaic performances.[10]

Recently the effect of crystal facet on the photocatalytic and photovoltaic performance has attracted much attention.[11,12] We have reported the first study on photocatalytic performance of anatase TiO_2 nanocrystals with a specific crystal facet on the surface and found that {010}-faceted anatase TiO_2 nanocrystals exhibit higher photocatalytic activity than the normal spherical nanocrystals without a specific facet on the surface.[13,14] The results encouraged researchers to study the effect of crystal facet on TiO_2 photocatalytic properties. Yang et al. have synthesized high percentage {001}-faceted TiO_2 particles using hydrofluoric acid solution; the results of their experimental study and first-principles quantum chemical calculation reveal that the {001}-facet of anatase is one of reactive facets for the photocatalytic reactions.[15] After that, Wu et al. have synthesized {010}-faceted and {001}-faceted anatase TiO_2 nanocrystals and found that the {010}-faceted nanocrystals exhibit higher photocatalytic activity than the {001}-faceted nanocrystals and commercial P25 sample in degradation of methyl orange.[16] The P25 sample is considered as a standard TiO_2 nanocrystal sample with high photocatalytic activity. Han et al. have reported that the {001}-faceted anatase TiO_2 nanosheets exhibit higher photocatalytic activity than the P25 sample.[17] Amano et al. have reported that {101}-faceted perfect

Received: July 15, 2014
Revised: September 18, 2014
Published: October 7, 2014

octahedral anatase crystallites exhibit higher photocatalytic activity than the P25 sample.[18] Therefore, these results indicate that in addition to bandgap and bulk band structure, the photocatalytic activity also depends on the crystal facet that relates both surface atomic structure and surface electronic band structure.[19−22]

The crystal facet also affects the DSSC performance. We have reported the first study on the crystal facet effect on the DSSC performance and found that {010}-faceted anatase nanocrystals exhibit specific high short-circuit current density (J_{sc}) due to strong adsorption of sensitizer dye molecules on the {010}-facet,[23,24] which improves injecting photoelectrons from LUMO (lowest unoccupied molecular orbital) of the molecule to the conduction band of TiO_2.[25] Wu et al. have reported that the bipyramid rod-like anatase nanocrystals with high percentage of {101} faces can capture the electrons injected from the dye photoexcited state to the anatase conducting band, decrease the annihilation of electrons, and increase the electron concentration of the TiO_2 photoelectrode compared with the spherical anatase nanocrystals.[26] The crystal facet effect on the DSSC performance has been confirmed also by other studies.[20,27−29]

Generally a hydrothermal process is used for the synthesis of the TiO_2 nanocrystals with a specific facet on the surface. The {001}-, {010}-, and {101}-faceted anatase nanocrystals have been synthesized by hydrothermal treatments of the titanium precursors in solutions containing hydrofluoric acid as a crystallographic controlling agent,[15,17] We have reported a unique and useful hydrothermal soft chemical process for the synthesis of {010}-facet anatase nanocrystals by topochemical conversion of layered titanate nanosheet precursors to anatase.[13,14,30,31]

However, the normal hydrothermal processes usually require a very long time, owing to late heat transmission in the normal hydrothermal processes. The microwave hydrothermal process is a unique and useful method, in which the solvent molecules and reactants can be heated directly by increasing their rotational speeds when solvent molecules and reactants absorb microwaves.[32] Some studies on microwave hydrothermal synthesis of TiO_2 nanocrystals have been reported. This unique heating process can shorten reaction time and increase the crystallization of products.[33−36] In the most cases, the TiO_2 nanocrystals with controllable crystal size and morphology were synthesized by microwave hydrothermal treatment of the colloidal TiO_2 solutions prepared by hydrolysis of the titanium compound.[32,35−38]

In this study, we describe synthesis of TiO_2 nanocrystals from exfoliated layered titanate nanosheet precursors with lepidocrocite-like structure using the microwave hydrothermal process for the first time. The microwave hydrothermal process can provide {010}-faceted anatase TiO_2 nanocrystals with uniform controllable sizes and morphologies. This gives us an opportunity to study the effects of crystal facet, size, and morphology on the bandgap, surface electronic band structure, photocatalytic activity, and DSSC performance of TiO_2 nanocrystals. The results revealed that the {010}-faceted anatase nanocrystals exhibit higher photocatalytic activity due to their larger bandgap and excellent DSSC performance compared with P25 nanocrystals, which contain [111]-faceted (facet vertical to [111]-direction) anatase nanocrystals and spherical anatase nanocrystals without a specific facet on the surface.

EXPERIMENTAL SECTION

Synthesis of HTO Layered Titanate Nanosheets Colloidal Solution. In this study, all reagents were used as received from Wako Pure Chemical Industries, unless otherwise stated. The layered titanate $K_{0.8}Ti_{1.73}Li_{0.27}O_4$ (KTLO) was synthesized by hydrothermal treatment of 5.1 g of KOH, 0.6 g of $LiOH{\cdot}H_2O$, and 6.9 g of TiO_2 (anatase form) in 25 mL of distilled water at 250 °C for 24 h under stirring conditions using a Hastelloy-C-lined vessel with internal volume of 45 mL. The obtained samples were washed to neutral with distilled water and dried in a drying oven to obtain the layered titanate KTLO as the precursor. The KTLO sample (10 g) was acid-treated with a 0.2 M HNO_3 solution (1 L) for 24 h under stirring conditions to exchange lithium ions and potassium ions with hydrogen ions to obtain a H^+-form layered titanate $H_{1.07}Ti_{1.73}O_4$ (HTO). The acid treatment was repeated again to ensure complete ion-exchange reaction. The HTO sample was washed with distilled water several times and then dried using a freeze drier. The HTO layered titanate nanosheet colloidal solution was prepared by treating 10 g of HTO sample in 0.1 M n-propylamine (PA; 1 L) solution under stirring conditions at room temperature for 24 h, and the HTO layered titanate nanosheet colloidal solution was named PA-HTO.

Microwave Hydrothermal Treatment of PA-HTO Solution. TiO_2 nanocrystals were prepared by microwave hydrothermal treatment of the PA-HTO nanosheet colloidal solution. Before the microwave hydrothermal treatment, the PA-HTO nanosheet colloidal solution was adjust to a desired pH value with a 3 M HCl solution in a pH range below 11.7 or a 1 M KOH solution in a pH range above 11.7. The pH adjusted PA-HTO solution (40 mL) was sealed into a Teflon vessel with internal volume of 80 mL, and then it was microwaved at a desired temperature for 2 h. After the microwave hydrothermal treatment, the obtained samples were washed with distilled water several times, and finally dried using a freeze drier. The obtained TiO_2 sample was named MW-*X*-*Y*, where *X* and *Y* were the temperature of microwave treatment and pH value of the nanosheet solution used for the microwave hydrothermal reaction, respectively.

Physical Analysis. The crystal structure of the samples was investigated using a powder X-ray diffractometer (Shimadzu, model XRD-6100) with Cu Kα (λ = 0.1542 nm) radiation. The size and morphology of the samples was characterized by field emission scanning electron microscopy (FE-SEM) (Hitachi, model S-900). Transmission electron microscopy (TEM) observation and selected-area electron diffraction (SAED) was performed on a JEOL model JEM-3010 system at 300 kV. Nitrogen gas adsorption was carried out on a QUANTACHROME AUTOSORB-1-MP apparatus. The specific surface area of samples was calculated from the adsorption data using the Brunauer−Emmett−Teller (BET) method.

Photocatalytic Characterization. A 20 mg sample of TiO_2 was added into a 10 ppm methylene blue aqueous solution (MB, 100 mL) and stirred for 2 h to disperse the sample well in the solution and to reach MB adsorption equilibrium on the TiO_2 nanocrystal surface under dark conditions without UV-irradiation. And then the suspension was illuminated by a 100 W ultraviolet lamp with 300−400 nm wavelength (UVA, Asahi Spectra, LAX-Cute) at room temperature with the lamp located 20 cm from the MB solution under continuously stirring conditions. At 20 min intervals, 3 mL of solution was drawn from the suspension and immediately centrifuged to separate the TiO_2 nanocrystals from the solution at 10000 rpm for 10 min. The MB concentration in the solution was determined by using a Shimadzu UV-2450 spectrophotometer. Degradation efficiency of MB by the photocatalytic reaction was calculated from the variations of the MB concentration in the solution before and after UV light irradiation.

Fabrication and Characterization of Dye-Sensitized Solar Cells. A TiO_2 nanocrystal paste was prepared by mixing TiO_2 nanocrystal sample (0.5 g), ethanol (2.5 g), α-terpineol (2.0 g), a 10 wt % solution of ethyl-cellulose 10 (8−14 mPa, 1.4 g), and a 10 wt % solution of ethyl-cellulose 45 (45−65 mPa, 1.1 g). The mixture was dispersed by ultrasonication for 30 min and then ball-milling for 72 h. After ball-milling, the ethanol was removed from the mixture using a rotary evaporator. P25 and ST20 nanocrystals paste were also prepared using a similar method. The P25 nanocrystal sample was purchased

dx.doi.org/10.1021/cg501062r | Cryst. Growth Des. 2014, 14, 5801−5811

from Degussa. The ST20 nanocrystal sample was synthesized by hydrothermal treatment of a commercial anatase nanoparticle sample (ST01, Ishihara Sangyo) with crystal size of 7 nm at 200 °C for 12 h.

The TiO_2 photoelectrode was prepared as follows. The fluorine-doped tin oxide (FTO) conducting glass plate was cleaned in distilled water and acetone by ultrasonication for 10 min, consecutively. Then the FTO glass plate was dipped in 0.1 M titanium tetraisopropoxide (TTIP) solution for 1 min and washed with distilled water and ethanol, dried at room temperature, and calcined at 480 °C for 1 h to coat the FTO glass surface with a dense TiO_2 thin film. The prepared TiO_2 paste was coated (10 mm × 10 mm) on the TTIP-treated FTO glass plates by a screen printing technique and kept in an ethanol box until the TiO_2 film surface was smooth and then dried at 120 °C for 10 min. This process was repeated to obtain a desired thickness of TiO_2 film. After the TiO_2 paste coating, the TiO_2 film was calcined at 450 °C for 30 min to obtain a TiO_2 porous electrode. The TiO_2 porous electrodes were dipped in the 0.1 M TTIP solution for 1 min, washed with distilled water and ethanol, dried at room temperature, and calcined at 480 °C for 1 h again. After cooling to 80 °C, the TiO_2 porous electrodes were soaked in a 3×10^{-4} M N719 dye (ditetrabutylammonium *cis*-bis(isothiocyanato)bis(2,2′-bipyridyl-4,4′-dicarboxylato)ruthenium(II)) solution for 24 h at room temperature and then washed with a t-butyl alcohol and acetonitrile (v/v = 50:50) mixed solvent.

The DSSCs were comprised of a dye-adsorbed TiO_2 electrode as an anode, a Pt-coated FTO glass as a cathode, and an electrolyte solution between the anode and the cathode. The electrolyte solution contained 0.1 M LiI, 0.01 M I_2, 0.6 M 1-butyl-3-n-propylimidazolium iodide (BMII), 0.4 M 4-*tert*-butylpyridine (TBP), and 0.1 M guanidine thiocyanate (GT) in acetonitrile and valeronitrile (v/v = 85:15). The photocurrent–voltage characteristic curves for the DSSCs were measured using a Hokuto-Denko BAS100B electrochemical analyzer under irradiation with simulated sunlight of AM 1.5 (100 mW/cm^2), using a sunlight simulator (YSS-E40, Yamashita Denso). A light-passing mask was fixed on the surface of FTO glass of the anode to set the effectively irradiating area on the cell as 0.25 cm^2.

RESULTS AND DISCUSSION

Microwave-Assisted Conversion of HTO Nanosheets to TiO_2 Nanocrystals. The PA-HTO nanosheet colloidal solutions with different pH values were hydrothermally microwaved at various temperatures to synthesize TiO_2 nanocrystals. The XRD patterns of samples prepared by hydrothermally microwaving the PA-HTO nanosheet solution at pH 11.5 at dissimilar temperatures are shown in Figure 1. Before the microwave hydrothermal treatment, PA-HTO has a lepidocrocite-like layered structure with a basal spacing of 1.09 nm (see Figure S1 in the Supporting Information), indicating $CH_3(CH_2)_2NH_3^+$ ($PA\text{-}H^+$) ions are intercalated into the interlayer space of HTO.[13,14] After the microwave hydrothermal treatment at 95 °C, a mixture of anatase phase and PA-HTO phase was obtained. With increasing temperature, the proportion of anatase phase increases and that of the PA-HTO phase decreases. At 165 °C, PA-HTO nanosheets were transformed to anatase phase completely, and single-phase anatase TiO_2 was obtained above this temperature. Meanwhile, the crystallinity of the formed anatase phase increases gradually with the temperature increase.

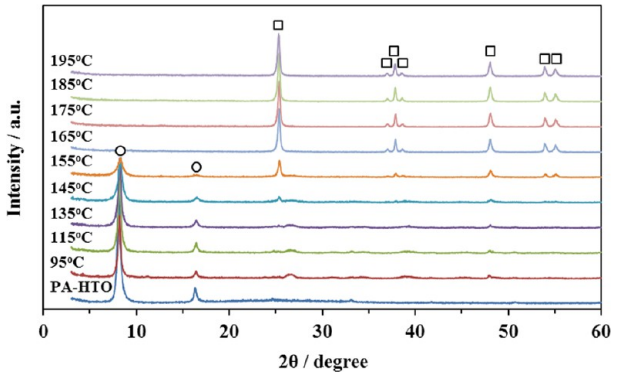

Figure 1. XRD patterns of PA-HTO nanosheet and products obtained by microwave hydrothermal treatment of PA-HTO nanosheet solution with pH 11.5 at different temperatures for 2 h. (○) PA-HTO phase; (□) anatase phase.

Figure 2 provides XRD patterns of products obtained by microwave hydrothermal treatment of PA-HTO nanosheet solutions at different pH values at 175 °C for 2 h. A mixture of rutile, brookite, and anatase phases was obtained at pH 0.5. In a pH range of 1.5 to 11.5, single-phase anatase TiO_2 was formed. The HTO layered phase is stable in a pH range of above 13, where $PA\text{-}H^+$ ions in the interlayer space and surface of HTO are exchanged with K^+ ions and then a K^+-form HTO phase with a basal spacing of 0.88 nm is formed, but it retains the lepidocrocite-like layered structure.[14] On the basis of the XRD results (see Figure S2 in the Supporting Information), the dependence of the products on the reaction temperature and pH value are summarized in Figure 3. The rutile and brookite phases are formed preferentially below pH 1, and anatase phase is formed preferentially in the pH range of 1 to 12. The

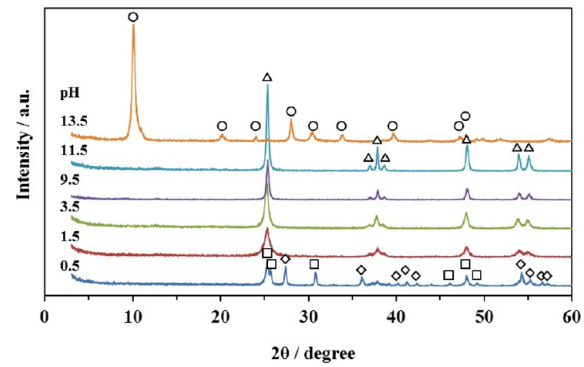

Figure 2. XRD patterns of products obtained by microwave hydrothermal treatment of PA-HTO nanosheet solutions with different pH values at 175 °C for 2 h: (○) K^+-form HTO phase; (△) anatase phase; (□) brookite phase; (◇) rutile phase.

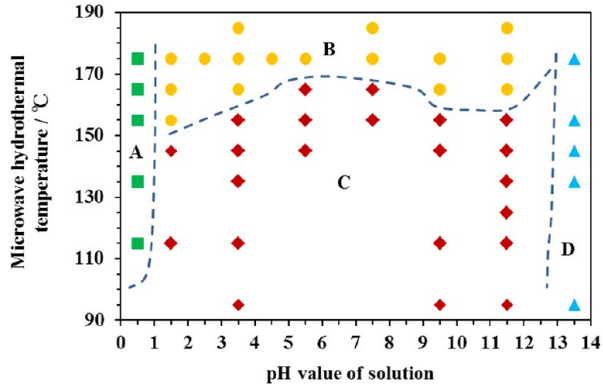

Figure 3. Phase diagram under microwave hydrothermal conditions: (A) mixture of rutile, brookite, and anatase phases; (B) anatase phase; (C) mixture of layered and anatase phases; (D) layered phase.

dx.doi.org/10.1021/cg501062r | *Cryst. Growth Des.* 2014, 14, 5801–5811

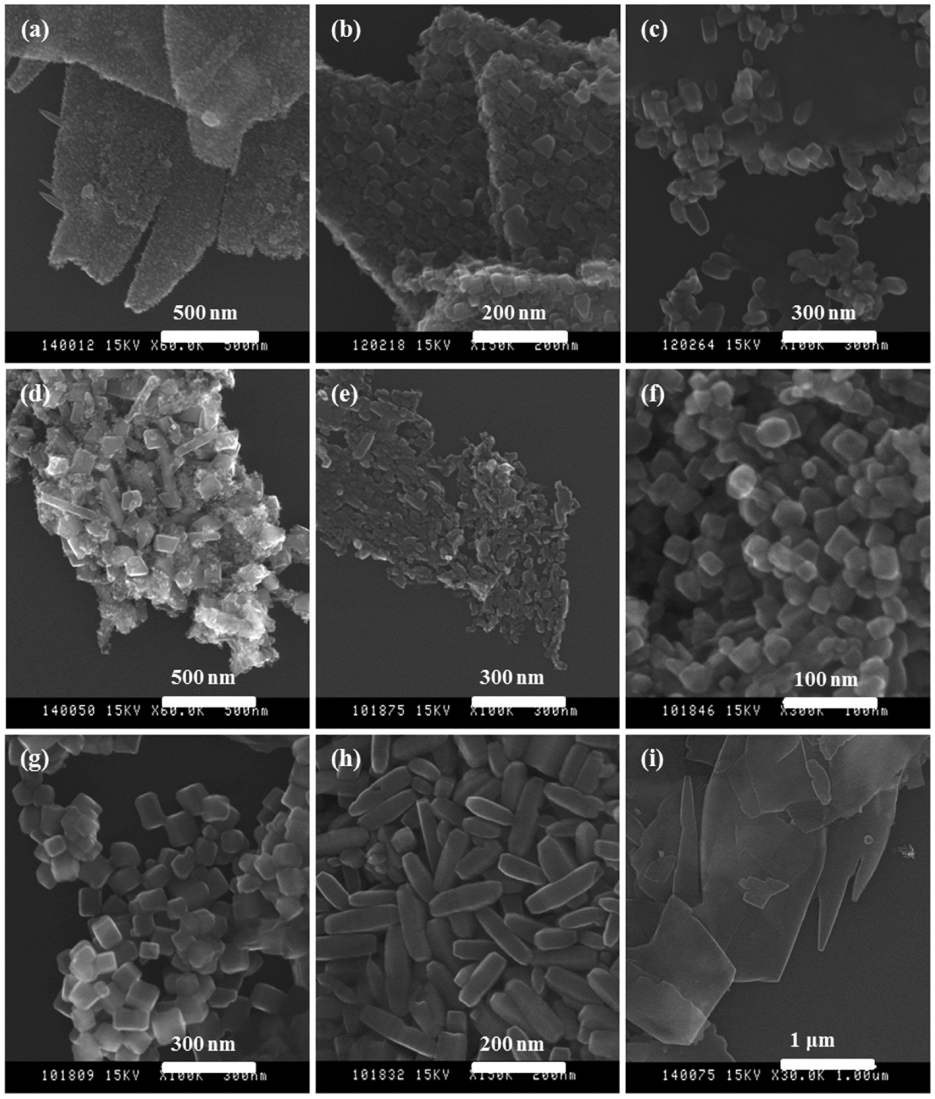

Figure 4. FE-SEM images of (a) MW-95-0.5, (b) MW-165-1.5, (c) MW-165-3.5, (d) MW-175-0.5, (e) MW-175-1.5, (f) MW-175-3.5, (g) MW-175-9.5, (h) MW-175-11.5, and (i) MW-175-13.5 samples.

lepidocrocite-like layered structure is stable in the pH range of above 13, where K^+-form HTO is formed. The result is different from normal hydrothermal treatment of HTO nanosheets, in which single-phase rutile is formed in the pH range below 1 and no brookite phase is formed in all pH range.[39] The formation of metastable brookite phase reveals that the microwave hydrothermal process is suitable for synthesis of such an unstable phase owing to its unique heating mechanism.[35,36] In comparison with normal hydrothermal treatment of PA-HTO solutions, the microwave hydrothermal process can significantly shorten reaction time and complete fast crystallization in a short period of time.[35,36]

Figure 4 shows FE-SEM images of the products obtained under different microwave hydrothermal conditions. MW-95-0.5 is a mixture of anatase and layered phases (see Figure S2a in the Supporting Information) and has a platelike particle morphology with a thickness about 50 nm (Figure 4a), which is much thicker than the PA-HTO nanosheet at about 1 nm (see Figure S3a in the Supporting Information). This result suggests that a restacking reaction of HTO nanosheets into the platelike particles occurs under the low pH conditions. Namely, PA-H^+ ions adsorbed on the HTO nanosheet surface are ion-exchanged with H^+ ions in the acidic solutions, which results in the restacking of the exfoliated HTO nanosheets. The platelike particle surface is covered with many small nanoparticles. The small nanoparticles correspond to the anatase phase. Platelike anatase particles with a thickness of about 30 nm were obtained at 165 °C and pH 1.5 (Figure 4b). The platelike particles are polycrystalline particles constructed from small nanocrystals with a size of about 20 nm. The platelike anatase particles are thicker than the HTO nanosheet, suggesting a restacking reaction of the HTO nanosheet during the conversion reaction from the HTO structure to the anatase structure under the low pH conditions. A mixture of platelike particles and tetragonal nanocrystals with a size of about 20 nm was obtained at 165 °C and pH 3.5 (Figure 4c). The XRD result indicates that this sample is single-phase anatase (see Figure S2f in the Supporting Information); therefore, the platelike and tetragonal nanocrystals are anatase phase. The formation of the platelike anatase particles can be explained by an in situ topochemical conversion reaction of HTO platelike particles to anatase platelike particles. The topochemical conversion reaction can retain particle morphology of the precursor after the structural transformation.[14,31] The formation of the small tetragonal

dx.doi.org/10.1021/cg501062r | *Cryst. Growth Des.* 2014, 14, 5801−5811

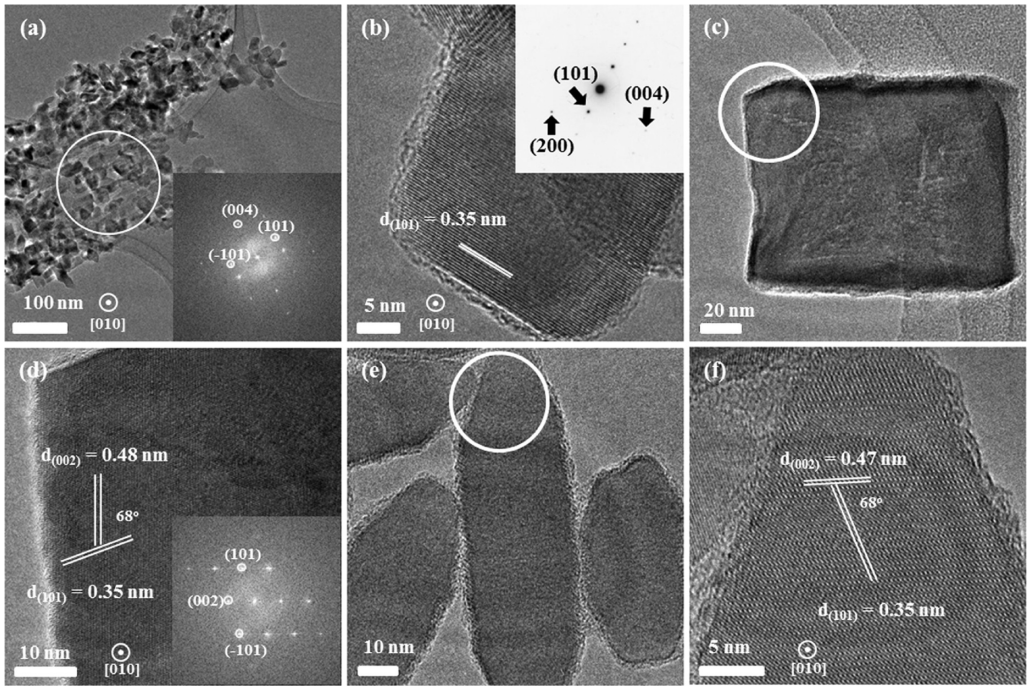

Figure 5. HR-TEM images, SAED, and Fourier transform (FTF) diffraction patterns of (a) MW-175-1.5, (b) MW-175-3.5, (c, d) MW-175-9.5, and (e, f) MW-175-11.5 samples.

anatase can be explained by splitting the platelike anatase particle to the small particles by a dissolution–deposition reaction on the platelike particle surface.

Three kinds of typical particle morphologies were observed in the MW-175-0.5 sample containing rutile, brookite, and anatase phases (Figure 4d). A TEM study reveals that the rodlike particles with a size of 300 nm in length and 50 nm in width correspond to the rutile phase, the block particles with a size of about 100 nm correspond to the brookite phase, and the nanocrystals with a size of about 20 nm correspond to anatase phase (see Figure S4 in the Supporting Information). The rutile, brookite, and anatase phases are formed mainly by the dissolution–deposition reaction mechanism similar to the normal hydrothermal reaction under the acidic reaction conditions because their particle morphologies have no relationship with the HTO nanosheet precursor.[40−42] At 175 °C and pH 1.5, the platelike anatase particle was almost split into nanocrystals with a size about 20 nm (Figure 4e), owing to increase of the dissolution–deposition reaction with increasing reaction temperature. At 175 °C and pH 3.5 (Figure 4f), tetragonal anatase nanocrystals with a size about 20 nm were observed, where no platelike anatase particles were observed. The average crystal size is similar to the small anatase crystals formed at 165 °C and pH 3.5, but the morphology is more uniform. The regular tetragonal anatase nanocrystals with size of about 80 nm were formed at 175 °C and pH 9.5 (Figure 4g). Regular quadratic prism anatase nanocrystals with a size of about 150 nm in length and 30 nm in width were formed at 175 °C and pH 11.5 (Figure 4h). These results reveal that the morphology and size controllable anatase nanocrystals can be prepared by changing the reaction temperature and the pH value of solution, and the crystal size increases with increasing pH value in a pH range of 3.5 to 11.5. The MW-175-13.5 sample with layered structure has platelike particle morphology (Figure 4i). The result reveals that HTO nanosheets are restacked into a platelike particles of K^+-HTO in the KOH solution and the layered structure is stable in the pH > 13 range under the microwave hydrothermal conditions.[14] Furthermore, compared with normal hydrothermal treatment of PA-HTO solutions (see Figure S5 in the Supporting Information), the microwave hydrothermal process can provide anatase nanocrystals with more uniform morphology and size, due to its uniform heating mechanisms.[39]

Nanostructural Study on Conversion Reaction from HTO Nanosheets to TiO_2 Nanocrystals. To understand the conversion reaction from HTO nanosheets to TiO_2 nanocrystals in detail, the synthesized nanocrystals were investigated using TEM and SAED (Figure 5). In MW-175-1.5, platelike particles constructed from nanocrystals with a size of about 20 nm are observed (Figure 5a). The platelike particle shows a Fourier transform (FTF) diffraction pattern of single crystal-like anatase phase with (101), (−101), and (004) planes. It indicates that all anatase nanocrystals in one platelike particle show same crystal orientation, and the [010]-direction is perpendicular to the basal plane of the platelike particle, namely, the (010)-faceted anatase mesocrystal was obtained. The transformation reaction from HTO nanosheets to anatase is a topochemical reaction, in which there is a specific crystallographic topological correspondence between the HTO structure and the anatase structure, where the [010]-direction of HTO corresponds to the [010]-direction of anatase, which are perpendicular to basal planes of the anatase platelike particle and HTO nanosheet (see Figure S3 in the Supporting Information).[31]

In MW-175-3.5, tetragonal nanocrystals were observed mainly. The typical tetragonal nanocrystal exhibits lattice fringes with a *d*-value of 0.35 nm corresponding to the (101) plane of anatase phase in its HR-TEM image, and diffraction spots of (101), (200), and (004) planes in its SAED pattern (Figure 5b). This result reveals that the [010]-direction is perpendicular to the basal plane of the tetragonal nanocrystal, namely, it is a (010)-faceted anatase nanocrystal exposing the

dx.doi.org/10.1021/cg501062r | *Cryst. Growth Des.* 2014, 14, 5801−5811

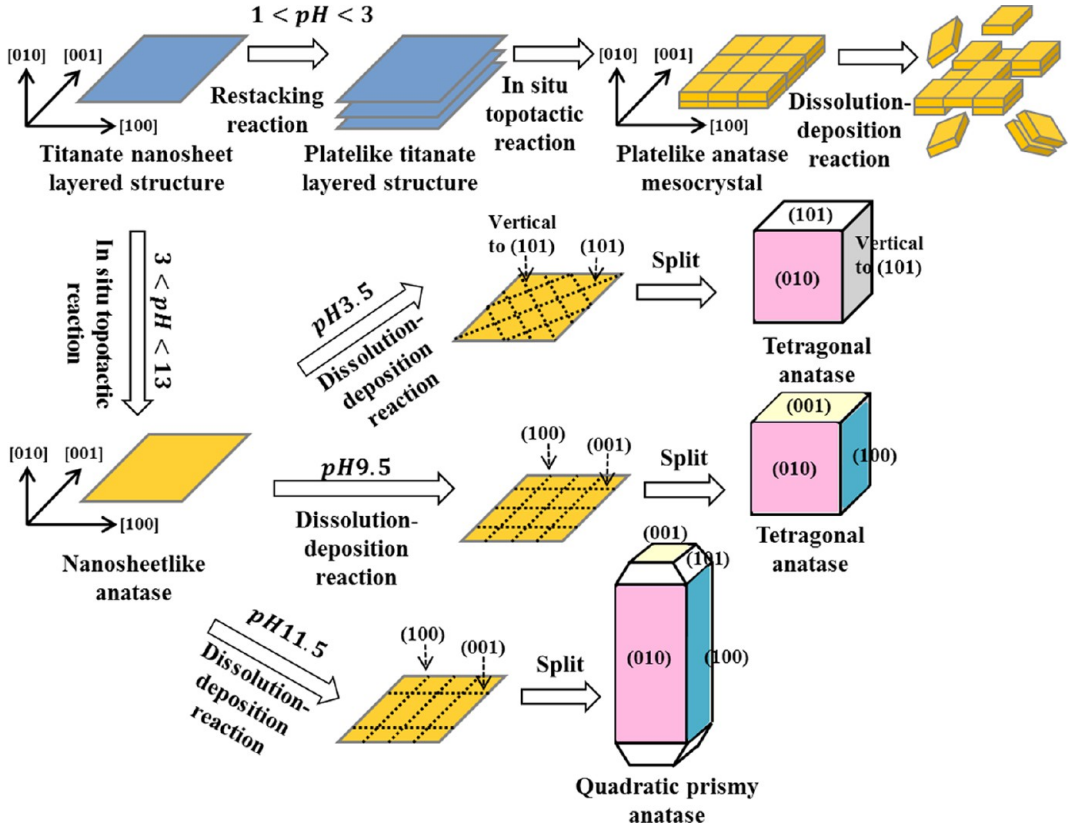

Figure 6. Transformation reaction mechanism from PA-HTO nanosheets to anatase TiO_2 nanocrystals.

(010) facet on the basal plane. And two side faces correspond to (101)-facets and other two side faces correspond to the facet vertical to (101) facet.

The (101) lattice fringes and (002) lattice fringes are observed in the HR-TEM images of tetragonal nanocrystal of MW-175-9.5 and quadratic prism nanocrystal of MW-175-11.5 (Figure 5c–f); that is, all these anatase nanocrystals prepared from the HTO nanosheets expose the (010)-facet on their basal planes. In the tetragonal nanocrystal of MW-175-9.5 and the quadratic prism nanocrystal of MW-175-11.5, two side faces correspond to (100)-facet and other two side faces to (001) facet, which are different from the tetragonal nanocrystal of MW-175-3.5. Furthermore, the axis direction of the quadratic prism nanocrystal corresponds to [001]-direction.

The above results are different from the results of normal hydrothermal reaction. Although all anatase nanocrystals prepared by treatment of HTO nanosheets under the normal hydrothermal conditions expose the (010)-facet on their basal planes, similar to the microwave hydrothermal treatment, the main product is rhombic anatase nanocrystals at pH 3.5, and only one kind of the tetragonal nanocrystal with two (101)-faceted side faces and other two side faces of the facet vertical to (101) facet is formed under the normal hydrothermal conditions.[39]

A reaction mechanism for the conversion reaction from the HTO nanosheets to TiO_2 nanocrystals can be summarized as in Figure 6 on the basis of the above results. In pH range of 1 to 3, first some PA-HTO nanosheets restack into platelike particles with a thickness of about 30 nm by ion-exchange of PA-H^+ ions adsorbed on the HTO nanosheet surface with H^+ ions in the solution. And then it is transformed into {010}-faceted platelike anatase particles via in situ topochemical conversion mechanism. The platelike anatase particle is constructed from well-aligned anatase nanocrystals in the {010}-orientation, namely, it is a {010}-faceted anatase mesocrystal. Furthermore, the anatase platelike mesocrystal can be split into its unit nanocrystals at high temperature by the dissolution–decomposition reaction.

In the pH range of 3 < pH < 13, first the PA-HTO nanosheet is transformed into {010}-faceted anatase nanosheet via in situ topochemical conversion reaction, and then the {010}-faceted anatase nanosheet can be split further into small anatase nanocrystals via the dissolution–decomposition reaction. Therefore, {010}-faceted anatase nanocrystals with tetragonal and quadratic prism morphologies can be formed. When the anatase nanosheets are split along the (101)-facet and the facet vertical to the (101)-facet, the tetragonal nanocrystals with two (101)-faceted side faces and two other side faces of the facet vertical to (101)-facet are formed (Figure 5b) at around pH 3.5. When the anatase nanosheets are split along the (100)-facet and the (001)-facet, the anatase nanosheet is split into the tetragonal nanocrystals with two (100)-faceted side faces and two (001)-faceted side faces (Figure 5d) at around pH 9.5 and to quadratic prism nanocrystals with two (100)-faceted side faces and two (001)-faceted side faces (Figure 5f) at around pH 11.5.

Furthermore, when the pH value is lower than 1, HTO can be transformed into rutile and brookite phases by the dissolution–decomposition reaction. Therefore, there are not correlations between the morphology of the HTO nanosheet precursor and rutile and brookite nanocrystals similar to the normal hydrothermal reaction. When the pH value is higher than 13, the HTO nanosheet is stable and maintains primary

dx.doi.org/10.1021/cg501062r | Cryst. Growth Des. 2014, 14, 5801–5811

morphology and structure under the microwave hydrothermal conditions.

The above results reveal that two main types of reactions can occur simultaneously in the formation reaction processes of the anatase nanocrystals from PA-HTO nanosheets. One is the in situ topotactic transformation reaction, in which the structure of PA-HTO nanosheets is transformed to anatase structure but the morphology of the precursor is retained after the reaction. Another is the dissolution−deposition reaction on the surface of the PA-HTO nanosheets, which splits the anatase nanosheet and platelike mesocrystal into small nanocrystals. And the nanocrystal morphology and size can be controlled by the dissolution−deposition reaction. The microwave hydrothermal process is suitable for controlling the dissolution−deposition reaction, owing to its uniform heating mechanism.

Electronic Band Structure and Photocatalytic Response of TiO_2 Nanocrystals. Since the facet on the TiO_2 crystal surface affects the photocatalytic activity, we investigated the photocatalytic activities of TiO_2 nanocrystals prepared from the PA-HTO nanosheets and also two other samples of P25 and ST20 for comparison. P25 is a benchmark TiO_2 nanocrystal sample commonly used in photocatalytic and DSSCs studies, owing to its high performance. P25 contains 80% anatase phase and 20% rutile phase. P25 contains about 80% of nanocrystals with a size of about 20 nm and about 20% of nanocrystals with a size about 80 nm (see Figure S6 in the Supporting Information). The nanocrystals with a size of about 20 nm are anatase phase, while those with a size of about 80 nm are rutile phase. There are two kinds of particle morphologies for the anatase nanocrystals. One is near-spherical morphology (content of about 40%), and the other is tetragonal morphology (content of about 40%). The near-spherical nanocrystals have no specific facet on the crystal surface, while tetragonal nanocrystals have a specific facet on the crystal surface. In the HR-TEM image of the tetragonal nanocrystal, the anatase lattice fringes of (101) and (011) (d = 0.352 nm) are observed. The HR-TEM image reveals that the basal plane of the tetragonal particle corresponds to a facet vertical to the [111]-direction (we call it as [111]-facet) and other four planes correspond to the {101}-facet as shown in Figure S6d in the Supporting Information. The [111]-facet is different from {111}-facet in the tetragonal system of anatase phase. The ST20 sample is anatase phase with spherical particle morphology without a specific facet on the surface and has a crystal size of about 20 nm (see Figure S6b in the Supporting Information).

Figure 7 shows the time-dependent photodegradation profiles of methylene blue (MB) dye over TiO_2 nanocrystals sample under ultraviolet irradiation. It can be seen that the photocatalytic activity increases in an order of ST20 < MW-175-11.5 < MW-175-1.5 < P25 < MW-175-3.5 < MW-175-9.5. It is well-known that the photocatalytic activity is strongly dependent on surface area of TiO_2 and is enhanced with increasing surface area. The measured specific surface area results are shown in Table 1. Although P25, ST20, and MW-175-3.5 have similar specific surface area values and similar crystal sizes of about 20 nm, MW-175-3.5 exhibits the highest photocatalytic activity in these three kinds of samples. This result implies that the {010}-facet exhibits higher photocatalytic activity than other facets. Although MW-175-9.5 has smaller specific surface area and larger crystal size than MW-175-3.5, it exhibits higher photocatalytic activity than MW-175-3.5. This result suggests that MW-175-9.5 has higher surface activity than

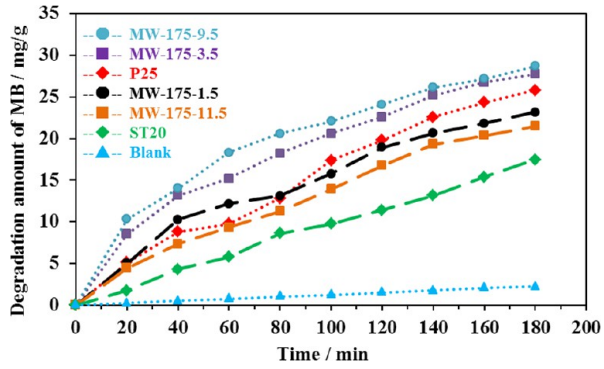

Figure 7. Photocatalytic degradation of methylene blue (MB) by MW-175-1.5, MW-175-3.5, MW-175-9.5, MW-175-11.5, P25, and ST20 samples.

that of MW-175-3.5. The higher surface activity might result from the larger faction of {010}-facet of MW-175-9.5, which has tetragonal morphology with four {010} planes and two {001} planes on its surface (Figure 6). MW-175-11.5 exhibits lower photocatalytic activity than that of MW-175-9.5, even though it has similar facets on the particle surface. This is owing to the smaller specific surface area and larger crystal size for MW-175-11.5. MW-175-1.5 exhibits photocatalytic activity less than MW-175-9.5 and MW-175-3.5 but higher than MW-175-11.5. Although the platelike mesocrystals of MW-175-1.5 have the smallest specific surface area, it exposes dominantly {010}-facets on the surface. This result also implies that the mesocrystal structure maybe enhances photocatalytic activity. P25 exhibits higher activity than ST20, suggesting that the activity of [111]-facet surface is higher than that of crystals without a specific facet. Therefore, the above results reveal that the surface photocatalytic activity is dependent on the facet exposed on the particle surface, ant it increases in an order of crystals without a specific facet < [111]-facet < (010)-facet.

To explain the surface photocatalytic activity order, we investigated the surface electronic band structures of the TiO_2 nanocrystals. The UV−visible absorption spectra of six kinds of TiO_2 samples are shown in Figure 8a. The absorption edges can be evaluated from the spectra as 385, 388, 390, 391.5, 395, and 397.5 nm for MW-175-3.5, MW-175-9.5, P25, MW-175-1.5, MW-175-11.5, and ST20, respectively. TiO_2 is an indirect semiconductor, and the relation between absorption coefficient (A) and incident photon energy ($h\nu$) can be represented as a Kubelka−Munk function $A = B(h\nu - E_g)^2/(h\nu)$, where B and E_g are the absorption constant and bandgap energy.[43] The bandgap energy was estimated from the transformed Kubelka−Munk function versus the energy of light (Figure 8b),[21,22] and the results are shown in Table 1. In the samples prepared from PA-HTO nanosheets, the bandgap increases in an order of MW-175-11.5 < MW-175-1.5 < MW-175-9.5 < MW-175-3.5, which corresponds to the average crystal size decrease order of MW-175-11.5 (150 nm) < MW-175-9.5 (90 nm) < MW-175-3.5 (20 nm), except the mesocrystal sample of MW-175-1.5. This can be explained by bandgap blue shift of nanocrystals with decreasing the crystal size.[20] Although MW-175-3.5, ST20, and P25 have almost same crystal size of about 20 nm, they show different bandgap values, which can be attributed to different facets on the particle surface. Namely, the (010)-facet has larger bandgap than the [111]-facet and the crystal without specific facet (spherical particle) on the surface. Although the {010}-faceted anatase mesocrystals of MW-175-1.5 are

dx.doi.org/10.1021/cg501062r | Cryst. Growth Des. 2014, 14, 5801−5811

Table 1. Crystal phase, Exposed Facet, Surface Area, Size, Absorption Edge, And Bandgap for TiO_2 Samples

sample	crystal phase	exposed facet	S_{BET} (m^2/g)	crystal size (nm)	absorption edge (nm)	E_g (eV)
P25	rutile/anatase	vertical to [111]	52.6	20	390	3.04
ST20	anatase	-	66.4	20	397.5	3.01
MW-175-1.5	anatase	(010)	13.5	-	391.5	3.03
MW-175-3.5	anatase	(010)	63.1	20	385	3.13
MW-175-9.5	anatase	(010)	33.2	80	388	3.05
MW-175-11.5	anatase	(010)	20.4	150	395	3.02

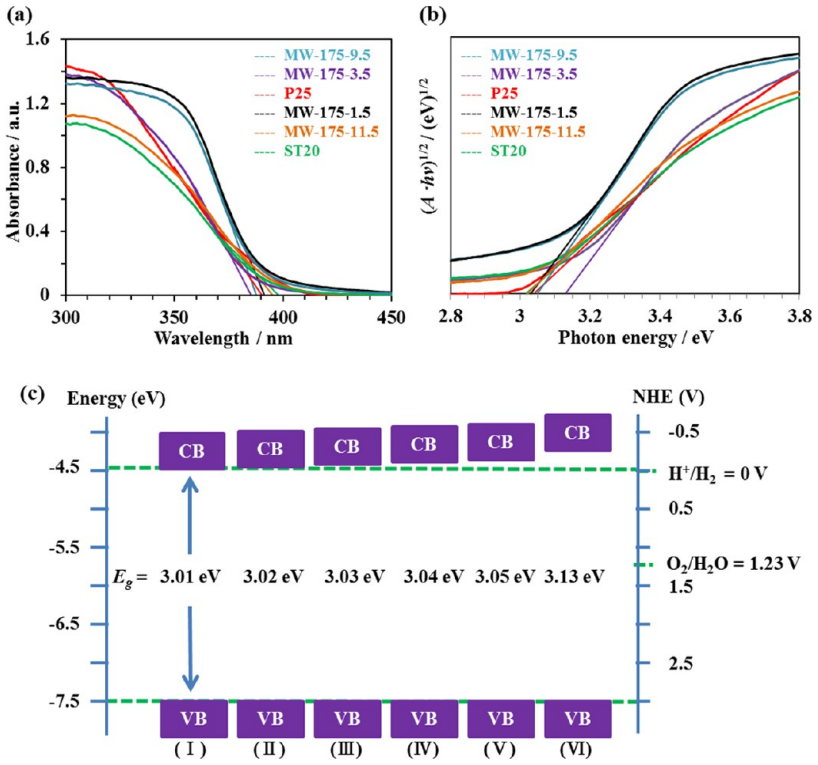

Figure 8. (a) UV−visible absorption spectra, (b) the corresponding plots of transformed Kubelka−Munk function versus the energy of photon, and (c) schematic illustration of the electronic band alignments of (I) ST20, (II) MW-175-11.5, (III) MW-175-1.5, (IV) P25, (V) MW-175-9.5, and (VI) MW-175-3.5 samples.

constructed from nanocrystals with size about 20 nm, its bandgap (3.03 eV) is much smaller than that (3.13 eV) of the (010)-faceted 20 nm nanocrystals of MW-175-3.5. This suggests that the blue shift effect decreases in the mesocrystal structure.

It has been reported that the energy levels of the highest valence band of anatase nanocrystals are similar even if they have different facets on the surface,[22] and the energy level of the highest valence band of anatase is evaluated as −7.5 eV.[44] Although P25 is a mixed phase of anatase and rutile, the photocatalytic activity is contributed mainly from the anatase phase because the principal component (80%) is anatase and anatase exhibits higher photocatalytic activity than rutile.[45] Furthermore, it has been reported that the energy level of highest valence band of P25 is almost same as that of anatase.[46] Therefore, the energy levels of the lowest conduction band and highest valence band for these six kinds of TiO_2 nanocrystals can be illustrated in Figure 8c by assuming that the energy levels of their highest valence bands are same at −7.5 eV and using the bandgap results of Figure 8b. The result reveals that the energy level of the conduction band increases in the order of ST20 < MW-175-11.5 < MW-175-1.5 < P25 < MW-175-9.5 < MW-175-3.5. This result suggests that the energy level of lowest conduction band of anatase increases in an order of crystal without a specific facet < [111]-facet < (010)-facet. In the photocatalytic reaction, the TiO_2 nanocrystals with a higher energy level of the lowest conduction band can generate more strongly reductive electrons for the photocatalytic reaction, which will show superior photocatalytic activity. Hence, the surface electronic band structure of the {010}-faceted anatase can provide high potential electrons for the photoreduction reaction. We think this is the reason the {010}-faceted anatase nanocrystals exhibit high surface photocatalytic activity.

DSSC Performance of TiO_2 Nanocrystals. We think that the surface electronic band structure of TiO_2 nanocrystals can affect also the DSSC performance, and therefore, we investigated the DSSC performance of the TiO_2 nanocrystals with different facets on the surface. The $I-V$ characteristics of DSSCs fabricated using anatase nanocrystals prepared from PA-HTO nanosheets, P25, and ST20 are shown in Figure 9. The DSSC parameters are given in Table 2. In the TiO_2 nanocrystals with similar crystal sizes of about 20 nm and different facets on the surface, the J_{sc} value increases in an order of ST20 (10.6 mA/cm^2) < P25 (13.3 mA/cm^2) < MW-175-3.5 (13.7 mA/cm^2). The V_{oc} value increases slightly in an order of MW-175-3.5 (0.66 V) < P25 (0.67 V) < ST20 (0.68 V), and

dx.doi.org/10.1021/cg501062r | Cryst. Growth Des. 2014, 14, 5801−5811

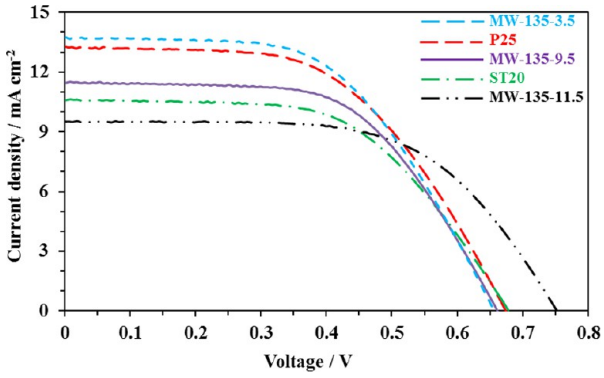

Figure 9. Current−voltage characteristic curves of DSSCs fabricated using MW-175-3.5, MW-175-9.5, MW-175-11.5, P25, and ST20 samples.

Table 2. Cell Performance Parameters of DSSCs Fabricated Using TiO_2 Samples

sample	J_{sc} (mA/cm^2)	V_{oc} (V)	ff	η (%)
P25	13.3	0.67	0.54	4.84
ST20	10.6	0.68	0.57	4.07
MW-175-3.5	13.7	0.66	0.55	4.97
MW-175-9.5	11.5	0.66	0.58	4.44
MW-175-11.5	9.54	0.75	0.60	4.32

the ff value increases slightly also in an order of P25 (0.54) < MW-175-3.5 (0.55) < ST20 (0.57). The η value increases in an order of ST20 (4.07%) < P25 (4.84%) < MW-175-3.5 (4.97%), which corresponds to the increasing order of the J_{sc} value. These results reveal that the η values are strongly dependent on the J_{sc} values, and MW-175-3.5 with the highest J_{sc} value gives the highest η value. The result suggests that the DSSC performance (η) is enhanced in the order of crystal without a specific facet < [111]-facet < {010}-facet, which corresponds to the increasing orders of the bandgap and the lowest energy level of conduction band (Figure 8c); that is, the DSSC performance is affected by the facet on the nanocrystal surface. It has been reported that the N719 dye adsorption constant K_{ad} on {010}-faceted anatase particles is larger than that on the [111]-faceted P25 nanocrystals and spherical nanocrystal surface without a specific facet, and the larger K_{ad}, namely, strong anchoring of the dye molecules onto the TiO_2 surface, can enhance J_{sc}.[24]

In the nanocrystals with the {010}-facet on the surface but different crystal sizes and morphologies, the J_{sc} value increases in an order of MW-175-11.5 (9.54 mA/cm^2) < MW-175-9.5 (11.5 mA/cm^2) < MW-175-3.5 (13.7 mA/cm^2), which corresponds to decreasing order of the crystal size. The V_{oc} value decreases in an order of MW-175-3.5 = MW-175-9.5 (0.66 V) ≪ MW-175-11.5 (0.75 V), and the ff value increases slightly in an order of MW-175-3.5 (0.55) < MW-175-9.5 (0.58) < MW-175-11.5 (0.60), which corresponds to the increasing order of crystal size. The increasing order of η value corresponds to the increasing order of J_{sc} value, MW-175-11.5 (4.32%) < MW-175-9.5 (4.44%) < MW-175-3.5 (4.97%). The above DSSC results reveal that the DSSC performance is affected not only by the facet on the particle surface but also by the crystal size and morphology. And the {010}-faceted anatase nanocrystals with size of about 20 nm are suitable for high performance DSSCs.

CONCLUSIONS

The {010}-faceted anatase nanocrystals with controllable crystal size and morphology and {010}-faceted anatase mesocrystal platelike particles can be synthesized by microwave hydrothermal treatment of PA-HTO nanosheet solutions. The sizes and morphologies of the TiO_2 nanocrystals strongly depend on the reaction temperature and pH value of the reaction solutions. There are two kinds of reactions in the formation process of the anatase nanocrystals. One is the in situ topochemical conversion reaction from PA-HTO nanosheet structure to anatase structure, and another is the dissolution−deposition reaction on the particle surface, which splits formed TiO_2 particles into small nanocrystals. The microwave hydrothermal process is suitable to control the crystal size and morphology due to its uniform heating mechanism. The UV−visible spectrum results reveal that the bandgap of the anatase nanocrystals is dependent on the facet exposed on the crystal surface and also the crystal size. The {010}-faceted anatase nanocrystal exhibits larger bandgap value than that of the [111]-faceted nanocrystal and spherical nanocrystal without a specific facet. The photocatalytic activities of the anatase nanocrystals are enhanced with increasing the bandgap. The DSSCs results for TiO_2 nanocrystals with different facets on the surface suggest that the J_{sc} and η values increase in the order of spherical nanocrystals without a specific facet < [111]-faceted nanocrystals < {010}-faceted nanocrystals; that is the {010}-faceted nanocrystals are promising for the high performance DSSCs.

ASSOCIATED CONTENT

Supporting Information

XRD patterns of KTLO, HTO, PA-HTO samples, and products obtained by microwave hydrothermal treatment at 95−185 °C, FE-SEM images, TEM and HR-TEM images of PA-HTO nanosheets, TEM and HR-TEM images of MW-175-0.5 sample, FE-SEM images of anatase nanoparticles obtained using normal hydrothermal treatment of PA-HTO nanosheet solutions at pH 3.5, 9.5, and 11.5, FE-SEM images of P25 and ST20 samples, and HR-TEM image and model of crystal facets on surface of tetragonal anatase nanocrystal of P25 sample. This material is available free of charge via the Internet at http://pubs.acs.org.

AUTHOR INFORMATION

Corresponding Author

*E-mail: feng@eng.kagawa-u.ac.jp.

Author Contributions

The manuscript was written through contributions of all authors. All authors have given approval to the final version of the manuscript.

Notes

The authors declare no competing financial interest.

ACKNOWLEDGMENTS

This work was supported in part by Grants-in-Aid for Scientific Research (B) (No. 26289240) from Japan Society for the Promotion of Science

REFERENCES

(1) Fujishima, A.; Honda, K. Electrochemical photolysis of water at a semiconductor electrode. *Nature* **1972**, *238*, 37−38.

(2) Fujishima, A.; Rao, T. N.; Tryk, D. A. Titanium dioxide photocatalysis. *J. Photochem. Photobiol. C* **2000**, *1*, 1−21.
(3) Nakata, K.; Fujishima, A. TiO_2 photocatalysis: Design and applications. *J. Photochem. Photobiol. C* **2012**, *13*, 169−189.
(4) O'Regan, B.; Grätzel, M. A low-cost, high-efficiency solar cell based on dye-sensitized colloidal TiO_2 films. *Nature* **1991**, *353*, 737−740.
(5) Grätzel, M. Photoelectrochemical cells. *Nature* **2001**, *414*, 338−344.
(6) Grätzel, M. Dye-sensitized solar cells. *J. Photochem. Photobiol. C* **2003**, *4*, 145−153.
(7) Asahi, R.; Morikawa, T.; Ohwaki, T.; Aoki, K.; Taga, Y. Visible-Light Photocatalysis in Nitrogen-Doped Titanium Oxides. *Science* **2001**, *293*, 269−271.
(8) Fujishima, A.; Zhang, X.; Tryk, D. A. TiO_2 photocatalysis and related surface phenomena. *Surf. Sci. Rep.* **2008**, *63*, 515−582.
(9) Zhang, S.; Yang, X.; Qin, C.; Numata, Y.; Han, L. Interfacial engineering for dye-sensitized solar cells. *J. Mater. Chem. A* **2014**, *2*, 5167−5177.
(10) Linsebigler, A. L.; Lu, G.; Yates, J. T., Jr. Photocatalysis on TiO_2 Surfaces: Principles, Mechanisms, and Selected Results. *Chem. Rev.* **1995**, *95*, 735−758.
(11) Sato, H.; Ono, K.; Sasaki, T.; Yamagishi, A. Frist-principles study of two-dimensional titanium dioxides. *J. Phys. Chem. B* **2003**, *107*, 9824−9828.
(12) Diebold, U. Structure and properties of TiO_2 surfaces: A brief review. *Appl. Phys. A: Mater. Sci. Process.* **2003**, *76*, 681−687.
(13) Wen, P.; Itoh, H.; Feng, Q. Preparation of Nanoleaf-like Single Crystals of Anatase-type TiO_2 by Exfoliation and Hydrothermal Reactions. *Chem. Lett.* **2006**, *35*, 1226−1227.
(14) Wen, P.; Itoh, H.; Tang, W.; Feng, Q. Single Nanocrystals of Anatase-Type TiO_2 Prepared from Layered Titanate Nanosheets: Formation Mechanism and Characterization of Surface Properties. *Langmuir* **2007**, *23*, 11782−11790.
(15) Yang, H. G.; Sun, C. H.; Qiao, S. Z.; Zou, J.; Liu, G.; Smith, S. C.; Cheng, H. M.; Lu, G. Q. Anatase TiO_2 single crystals with a large percentage of reactive facets. *Nature* **2008**, *453*, 638−641.
(16) Wu, B.; Guo, C.; Zheng, N.; Xie, Z.; Stucky, G. D. Nonaqueous Production of Nanostructures Anatase with High-Energy Facets. *J. Am. Chem. Soc.* **2008**, *130*, 17563−17567.
(17) Han, X.; Kuang, Q.; Jin, M.; Xie, Z.; Zheng, L. Synthesis of Titania Nanosheets with a High Percentage of Exposed (001) Facets and Related Photocatalytic Properties. *J. Am. Chem. Soc.* **2009**, *131*, 3152−3153.
(18) Amano, F.; Yasumoto, T.; Prieto-Mahaney, O.-O.; Uchida, S.; Shibayama, T.; Ohtani, B. Photocatalytic Activity of Octahedral Single-Crystalline Mesoparticles of Anatase titanium (IV) Oxide. *Chem. Commun.* **2009**, *17*, 2311−2313.
(19) Pan, J.; Liu, G.; Lu, G.; Cheng, H. On the True Photoreactivity Order of {001}, {010}, and {101} Facets of Anatase TiO_2 crystals. *Angew. Chem., Int. Ed.* **2011**, *50*, 2133−2137.
(20) Pan, J.; Wu, X.; Wang, L.; Liu, G.; Lu, G.; Cheng, H. Synthesis of Anatase TiO_2 Rods with Dominant Reactive {010} Facets for the Photoreduction of CO_2 to CH_4 and Use in Dye-Sensitized Solar Cells. *Chem. Commun.* **2011**, *47*, 8361−8363.
(21) Xu, H.; Ouyang, S.; Li, P.; Kako, T.; Ye, J. High-Active Anatase TiO_2 Nanosheets Exposed with 95% {100} Facets toward Efficient H_2 Evolution and CO_2 Photoreduction. *ACS Appl. Mater. Interfaces* **2013**, *5*, 1348−1354.
(22) Xu, H.; Reunchan, P.; Ouyang, S.; Tong, H.; Umezawa, N.; Kako, T.; Ye, J. Anatase TiO_2 Single Crystals Exposed with High Reactive {111} Facets toward Efficient H_2 Evolution. *Chem. Mater.* **2013**, *25*, 405−411.
(23) Wen, P.; Tao, Z.; Ishikawa, Y.; Itoh, H.; Feng, Q. Dye-Sensitized Solar Cells Based on Anatase TiO_2 Nanocrystals Exposing a Specific Lattice Plane on the Surface. *Appl. Phys. Lett.* **2010**, *97*, No. 131906.
(24) Wen, P.; Xue, M.; Ishikawa, Y.; Itoh, H.; Feng, Q. Relationships between Cell Parameters of Dye-Sensitized Solar Cells and Dye-Adsorption Parameters. *ACS Appl. Mater. Interfaces* **2012**, *4*, 1928−1934.
(25) Hagfeldt, A.; Boschloo, G.; Sun, L.; Kloo, L.; Pettersson, H. Dye-Sensitized Solar Cells. *Chem. Rev.* **2010**, *110*, 6595−6663.
(26) Wu, J.; Hao, S.; Lin, J.; Huang, M.; Huang, Y.; Lan, Z.; Li, P. Crystal Morphology of Anatase Titania Nanocrystals Used in Dye-Sensitized Solar Cells. *Cryst. Growth Des.* **2008**, *8*, 247−252.
(27) Yang, W.; Wang, Y.; Shi, W. One-Step Synthesis of Single-Crystal Anatase TiO_2 Tetragonal Faceted-Nanorods for Improved-Performance Dye-Sensitized Solar Cells. *CrystEngComm* **2012**, *14*, 230−234.
(28) Shiu, J.-W.; Lan, C.-M.; Chang, Y.-C.; Wu, H.-P.; Huang, W.-K.; Diau, E. W-G. Size-Controlled Anatase Titania Single Crystals with Octahedron-like Morphology for Dye-Sensitized Solar Cells. *ACS Nano* **2012**, *6*, 10862−10873.
(29) Shen, P.-S.; Tai, Y.-C.; Chen, P.; Wu, Y.-C. Clean and Time-Effective Synthesis of Anatase TiO_2 Nanocrystalline by Microwave-Assisted Solvothermal Method for Dye-Sensitized Solar Cells. *J. Power Sources* **2014**, *247*, 444−451.
(30) Wen, P.; Itoh, H.; Tang, W.; Feng, Q. Transformation of Layered Titanate Nanosheets into Nanostructured Porous Titanium Dioxide in Polycation Solution. *Microporous Mesoporous Mater.* **2008**, *116*, 147−156.
(31) Wen, P.; Ishikawa, Y.; Itoh, H.; Feng, Q. Topotactic Transformation Reaction from Layered Titanate Nanosheets into Anatase Nanocrystals. *J. Phys. Chem. C* **2009**, *113*, 20275−20280.
(32) Corradi, A. B.; Bondioli, F.; Focher, B. Conventional and Microwave-Hydrothermal Synthesis of TiO_2 Nanopowders. *J. Am. Ceram. Soc.* **2005**, *88*, 2639−2641.
(33) Komarneni, S.; Roy, R.; Li, Q. H. Microwave-Hydrothermal Synthesis of Ceramic Powders. *Mater. Res. Bull.* **1992**, *27*, 1393−1405.
(34) Komarneni, S.; Rajha, R. K.; Katsuki, H. Microwave-Hydrothermal Processing of Titanium Dioxide. *Mater. Chem. Phys.* **1999**, *61*, 50−54.
(35) Wilson, G. J.; Will, G. D.; Frost, R. L.; Montgomery, S. A. Efficient Microwave Hydrothermal Preparation of Nanocrystalline Anatase TiO_2 Colloids. *J. Mater. Chem.* **2002**, *12*, 1787−1791.
(36) Wilson, G. J.; Matijasevich, A. S.; Mitchell, D. R. G.; Schulz, J. C.; Will, G. D. Modification of TiO_2 for Enhanced Surface Properties: Finite Ostwald Ripening by a Microwave Hydrothermal Process. *Langmuir* **2006**, *22*, 2016−2027.
(37) Wang, H. E.; Zheng, L. X.; Liu, C. P.; Liu, Y. K.; Luan, C. Y.; Cheng, H.; Li, Y. Y.; Martinu, L.; Zapien, J. A.; Bello, I. Rapid microwave synthesis of porous TiO2 spheres and their applications in dye-sensitized solar cell. *J. Phys. Chem. C* **2011**, *115*, 10419−10425.
(38) Manseki, K.; Kondo, Y.; Ban, T.; Sugiura, T.; Yoshida, T. Size-controlled synthesis of anisotropic TiO_2 single nanocrystals using microwave irradiation and their application for dye-sensitized solar cells. *Dalton Trans.* **2013**, *42*, 3295−3299.
(39) Chen, C.; Sewvandi, G. A.; Kusunose, T.; Tanaka, Y.; Nakanishi, S.; Feng, Q. Synthesis of {010}-Faceted Anatase TiO_2 Nanoparticles from Layered Titanate for Dye-sensitized Solar Cells. *CrystEngComm* **2014**, *16*, 8885−8895.
(40) Zheng, Y.; Shi, E.; Chen, Z.; Li, W.; Hu, X. Influence of Solution Concentration on the Hydrothermal Preparation of Titania Crystallites. *J. Mater. Chem.* **2001**, *11*, 1547−1551.
(41) Feng, X.; Zhai, J.; Jiang, L. The Fabrication and Switchable Superhydrophobicity of TiO_2 Nanorod Films. *Angew. Chem., Int. Ed.* **2005**, *44*, 5115−5118.
(42) Li, G.; Gray, K. A. Preparation of Mixed-phase Titanium Dioxide Nanocomposites via Solvothermal Processing. *Chem. Mater.* **2007**, *19*, 1143−1146.
(43) Butler, M. A. Photoelectrolysis and Physical Properties of the Semiconducting Electrode WO_2. *J. Appl. Phys.* **1977**, *48*, 1914−1920.
(44) Nakamura, R.; Tanaka, T.; Nakato, Y. Mechanism for Visible Light Responses in Anodic Photocurrents at N-Doped TiO_2 Film Electrodes. *J. Phys. Chem. B* **2004**, *108*, 10617−10620.
(45) Carp, O.; Huisman, C. L.; Reller, A. Photoinduced Reactivity of Titanium Dioxide. *Prog. Solid State Chem.* **2004**, *32*, 33−177.

(46) Martin, S. T.; Herrmann, H.; Hoffmann, M. R. Time-resolved Microwave Conductivity Part 2.-Quantum-sized TiO_2 and the Effect of Adsorbates and Light Intensity on Charge-carrier Dynamics. *J. Chem. Soc., Faraday Trans.* **1994**, *90*, 3323−3330.